Computational Analysis of Structure and Binding Energy for the Development of a Cisplatin-Loaded Protein Nanocarrier

Søren C. Spina[1], Joe Bailey[1], Blaise Kimmel[1-3,*]

[1]Department of Chemical and Biomolecular Engineering, The Ohio State University, Columbus, OH, 43210, United States
[2]Center for Cancer Engineering, Ohio State University Comprehensive Cancer Center, The Ohio State University, Columbus, OH, 43210, United States
[3]Pelotonia Institute for Immuno-Oncology, Ohio State University Comprehensive Cancer Center, The Ohio State University, Columbus, OH, 43210, United States

*To whom correspondence should be addressed

Corresponding Author
Blaise R. Kimmel, Ph.D.
151 W. Woodruff Avenue Columbus, OH 43210
Email: kimmel.85@osu.edu

Lay Abstract

This study provides a computational approach to quantify cisplatin binding to platinum-coordinating amino acids. We study potential cisplatin-binding sites within a model MSH6 protein carrier, and evaluate cisplatin's mechanism of action at the DNA level. Our results inform the strategic design of protein nanocarriers for targeted cisplatin delivery.

Scientific Abstract

Platinum-based drugs, such as cisplatin, are first-line chemotherapy treatments for patients with cancer. However, the success of these drugs is balanced with severe off-target toxicities and high dosing requirements, prompting the development of selective nanocarriers for targeted drug delivery. This study uses a computationally guided approach to examine the role that amino acids play in cisplatin binding for the potential to generate a protein nanocarrier. Using density functional theory, we quantify the binding of cisplatin to platinum-coordinating amino acids. We then rationally engineer a model MSH6 protein carrier, and evaluate the ability of MSH6 to bind cisplatin via molecular docking simulations. Structure predictions of the engineered MSH6 show that inserting the cisplatin-binding site has a limited impact on the nearby protein architecture of MSH6. Finally, we confirm and reveal cisplatin's mechanism of action with DNA binding, and compare the energetic potentials of DNA binding from protein-delivered cisplatin to systemically administered cisplatin. Future studies will use these results to experimentally validate the binding of cisplatin in model protein carriers, and inform the strategic design and experimental development of a protein nanocarrier to achieve targeted drug delivery in cancer.

Introduction

Cisplatin and platinum-based derivatives have been used to treat a wide range of cancer types, being a first-in-line treatment option for many sarcomas and carcinomas[1]. When systemically administered to a patient, the amino groups typically enable cisplatin to enter cells via passive diffusion. In the cytoplasm, the amino groups of cisplatin undergo aquation, replacing the two bound chlorine atoms, forming dihydroxo moieties. In its water-soluble form, cisplatin exerts its chemotherapeutic action by crosslinking two purine bases on a DNA strand, causing irreparable damage that leads to cell death (**Figure 1**). Although cisplatin is highly effective at inducing apoptosis in tumor cells, systemic administration results in off-target cellular delivery, leading to DNA damage and toxicities in healthy tissues, especially those of the heart, liver, kidney, and hearing systems[2]. Many platinum-containing derivatives have been developed to exhibit potent anti-tumor effects via DNA damage, yet there remains a need for therapeutics that enhance the on-target delivery of these molecular agents.

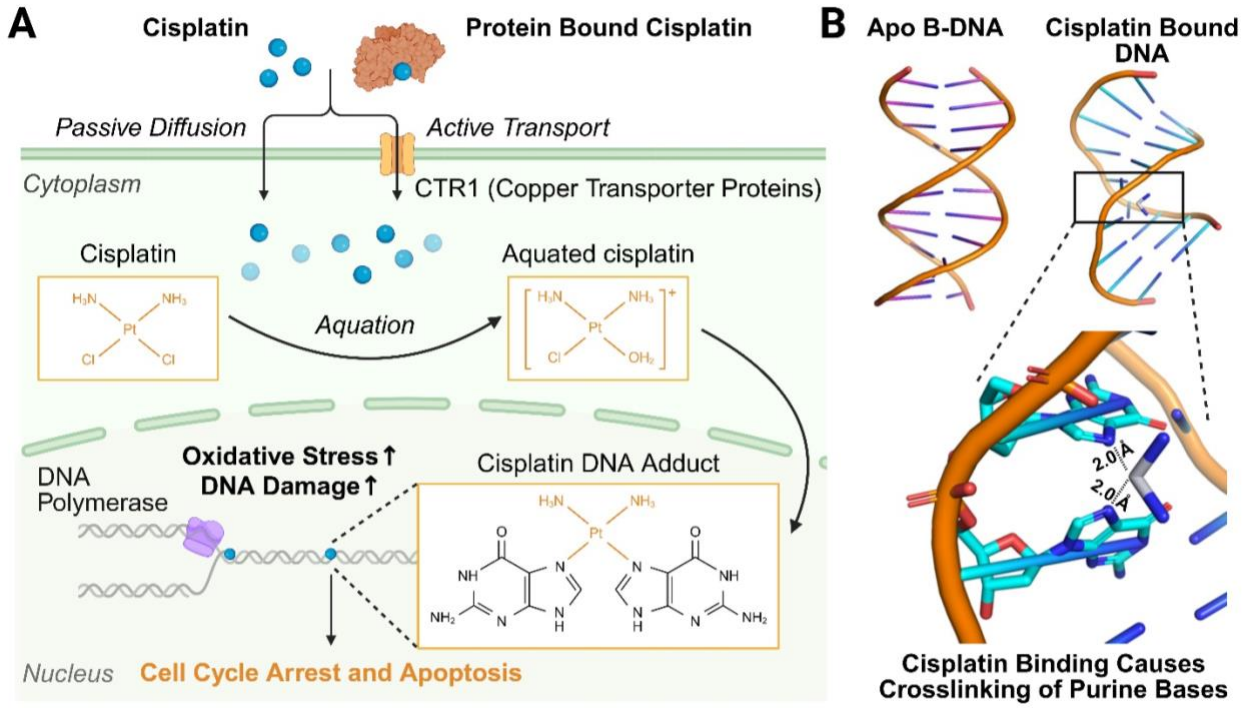

Figure 1. Cisplatin's mechanism of action. (A) Cisplatin enters the cell via passive diffusion or active transport, undergoes aquation inside the cell, and forms a DNA adduct by (B) crosslinking purine bases, which can create bends (PDB: 1KSB) in straight DNA (PDB: 1AGH). Molecular visualization was performed with PyMOL.

Protein- and peptide-based therapeutics have recently gained popularity as potential vehicles for targeted delivery of molecular agents to treat cancer, including immune-activating drugs and chemotherapies, which have demonstrated significant improvements in on-target tumor delivery and reduced off-target toxicities in preclinical and clinical trials[3]. By combining the selectivity of a protein therapy with the cytotoxicity of cisplatin, a selective and reliable cancer treatment could be developed for translation into the clinic. Supported by recent work in the field, apo-Human serum transferrin has been shown to improve tumor-specific delivery of cisplatin to human hepatocellular liver carcinoma cells *in vitro*, leading to apoptosis[4,5]. Historically, human serum albumin (known for a long half-life in circulation) and the copper efflux transporter ATP7B have been observed binding to and transporting cisplatin to cells, where cisplatin is able to enter cells via passive or active diffusion, relying on cellular transport proteins (e.g., CTR1, copper transporter proteins) (**Figure 1A**)[6]. While these examples demonstrate cisplatin's ability to form a covalent adduct with proteins, there is a knowledge gap in predicting the binding site of cisplatin on candidate protein carriers and the residue to which it reacts, limiting the rational design of protein-drug conjugates for targeted cisplatin delivery.

This work addresses this gap by providing a computational investigation into how a biologic nanocarrier, at both the amino acid and protein level, plays a direct role in active cisplatin transport. We evaluate the simulating binding interactions of key residues associated with cisplatin binding – histidine, lysine, methionine, arginine, cysteine, aspartate, and glutamate – to model cisplatin-protein binding via coordination of the platinum [II] ion. From these calculations, we rationally engineer a cisplatin-binding site into human MSH6, a model protein that binds to MSH2, thereby completing the formation of the MutSα complex[7]. We use computational chemistry (via Density Functional Theory, DFT) calculations to study cisplatin binding and crosslinking purine nucleobases to understand how cisplatin then interacts with DNA, along with the role of aquation. Collectively, our study simulates and models the interactions between cisplatin and amino acids within a model protein, positioning cisplatin delivery as a therapeutic strategy via rational protein design.

Computational Methods

Cisplatin-Biomolecule Binding Calculations Using DFT

Modeling was completed in Avogadro 2, where an initial geometry optimization was completed using Babel [8]. A full geometry optimization and frequency calculation was then performed in ORCA [9,10] using the close-shell restricted hybrid density functional B3LYP method with the SMD solvation model [11]. For organic atoms, the 6-31+G(d,p) basis set was used. For the platinum atom, the def2-TZVP basis set with def2-ECP was used. A fine grid was used for numerical integration. Each multiplicity was set to 1, and the SCF was set as tight. The thermodynamics of cisplatin, monosubstituted aqua cisplatin, and disubstituted aqua cisplatin, binding amino acids, nucleobases, and were calculated. The following equation was used to determine the total electronic energy (ΔE) and total free energy (ΔG).

$$\Delta E = E(\textit{complex}) + E(\textit{Chlorine/Water}) - E(\textit{cisplatin}) - E(Amino\ Acid/\ Nucleic\ Acid)$$

$$\Delta G = G(\textit{complex}) + G(\textit{Chlorine/Water}) - G(\textit{cisplatin}) - G(Amino\ Acid/\ Nucleic\ Acid)$$

In Silico Mutagenesis, Molecular Docking, and Structural Prediction of Engineered MSH6

The experimental structure of the human MSH6 (PDB: 2O8B) was obtained from the Protein Data Bank and visualized using PyMOL version 3.0[12]. Four residues (450-453) of the DNA-interaction site were mapped and mutated to engineer a cisplatin binding site. Mutations include V450K F451E M452C K453H. For each mutation, the rotamer of the lowest strain value was selected. MetalDock was used to dock cisplatin against the engineered MSH6 structure. The pH was set to 7.5, with grid coordinates of the docking box being 46, 46, 36 and a box size of 19, 20, 20. Boltz-2, within the Tamarind Bio webserver, was used to predict the structures of engineered and wild-type MSH6. Each structure was aligned with the MSH6 crystal structure (PDB: 2O8B) using the PyMOL alignment tool.

Results

Thermodynamics of Loading Cisplatin onto Amino Acids

We calculated and compared the binding abilities of individual amino acids to inform the rational design and generation of a cisplatin-binding pocket (**Figure 2**). Through observance of protein-cisplatin structures available on the protein data bank, histidine, lysine, methionine, cysteine, arginine, aspartate, and glutamate are the amino acids that directly coordinate the platinum atom

of cisplatin. We used density functional theory with a B3LYP method within the ORCA program to calculate the electronic energy (E) and free energy (G) of amino acid-cisplatin complex formation. We performed these calculations with cisplatin, monosubstituted aqua cisplatin, and disubstituted cisplatin to better inform the creation of a cisplatin binding site with tunable strength regarding aquation (**Tables 1-3**).

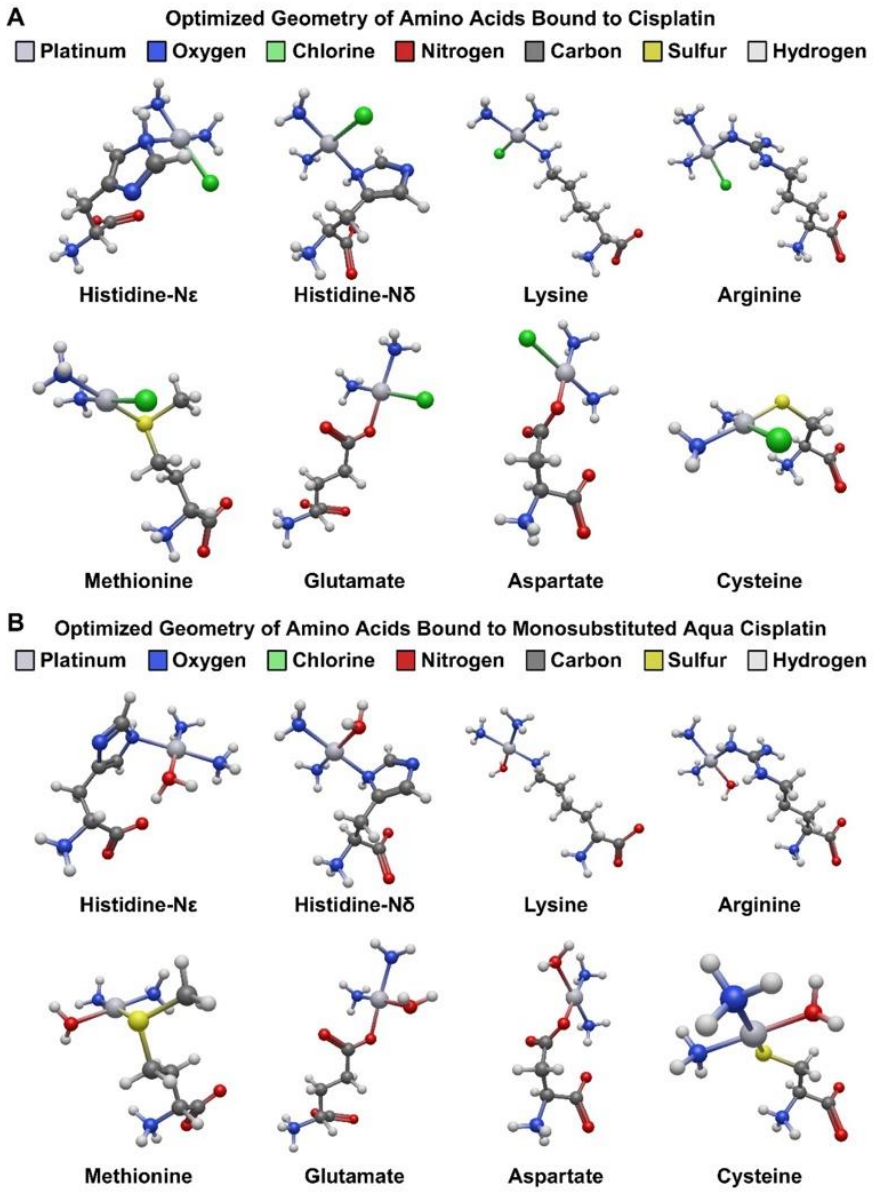

Figure 2. Geometrically optimized structures of cisplatin-binding amino acids. Input and output structures were modeled in Avogadro 2. Geometry optimization was performed with ORCA via the restricted B3YLP method using a def2-TZVP basis set for platinum atoms and the 6-31+G(d,p) basis set for organic atoms.

Histidine is the most prevalent ligand of cisplatin in structures deposited in the protein data bank. The platinum ion can coordinate to nitrogen at both the Nε and Nδ positions[13]. We calculated that cisplatin binding, regardless of aquation status, was significantly more thermodynamically favorable at the ε-nitrogen than at the δ-nitrogen. This is likely due to steric interference of the protein chain on the residues. Histidine can bind cisplatin in a wide range of nitrogen-based coordination chemistries. With this in mind, and after analyzing the dynamic free energy results as aquation proceeds, we hypothesized that coordination to histidine is tunable depending on the nitrogen-binding site and the level of aquation. Further, this hypothesis is driven by the observation that histidine shares a functional group with the purine moiety in known cisplatin nucleobase binders, providing a potential analogue to examine thermodynamic differences in cisplatin coordination to the delta and epsilon nitrogen atoms of histidine.

Cysteine has been shown to coordinate cisplatin clusters, such as with the human copper chaperone, by four cysteine residues[14]. After calculating the binding energy of cisplatin to cysteine, we found that it had the most thermodynamically favorable binding out of the amino acids tested. It bound disubstituted aqua cisplatin most strongly with an electronic energy and free energy that is ~2x that of cisplatin and monosubstituted cisplatin. The trend of cysteine favoring the disubstituted aqua cisplatin is consistent with previous computational studies[15]. Experimentally validated binding studies show that cysteine coordinates cisplatin with a much stronger interaction than methionine. The other sulfur-containing amino acid, methionine, is documented to coordinate cisplatin.

In previous studies, it has been shown that the thiol group of cysteine binds to cisplatin via charge transfer from the sulfur to the platinum atom in the shared covalent bond[15]. While this interaction has been found to be strong for cysteine, similar reports from this work have suggested comparable ionic bonding between the sulfur atom in methionine and platinum. Further, some studies report that sulfur binding can induce ammonia release from the platinum [II] ion via the strong sulfur trans effect and trans influence, leaving cisplatin inactivated[16]. Our work expanded on this, examining the chemical thermodynamics of bond coordination and electron density transfer between these sulfur atoms to platinum. Here, our DFT results suggest that cysteine coordination proceeds with a higher thermodynamic stability ($\Delta G_{rxn,Cys}$ = -10.5823 kcal/mol) compared to that of methionine coordination ($\Delta G_{rxn,Met}$ = 7.08282 kcal/mol) (**Table 1**).

Lysine has been shown to bind cisplatin in *Plasmodium falciparum* parasites, forming a reduced glutaredoxin 1 complex, as well as in thaumatin and human heavy chain ferritin[17,18]. Lysine, Aspartate, and glutamate are similar amino acids that have been experimentally shown to coordinate cisplatin via an oxygen atom. These electrophilic atoms within the residue were expected to likely pair well due to the nucleophilic effects of the cisplatin binding to DNA. Aspartate and glutamate follow similar trends of binding, becoming thermodynamically favorable only when reacting with disubstituted aqua cisplatin.

Amino Acid + Cisplatin → Cisplatin-AA + Chloride			
	ΔE_{rxn}(kcal/mol)	**ΔH_{rxn}(kcal/mol)**	**ΔG_{rxn}(kcal/mol)**
Arginine	15.14681	18.32766	24.31409
Aspartate	-0.26795	1.009034	6.677323
Cysteine	-16.4483	-15.4486	-10.5823
Glutamate	-1.20369	1.046999	5.659064
Histidine-Nε	24.30487	25.3491	30.92176
Histidine-Nδ	-1.20369	1.046999	5.659064
Lysine	-8.68322	-6.83702	0.169302
Methionine	-0.91554	0.625062	7.08282

Table 1. Calculated thermodynamics for an amino acid binding cisplatin. Inputs were modeled in Avogadro 2 and then geometrically optimized with a frequency calculation in ORCA via the restricted B3YLP method using a def2-TZVP basis set for platinum atoms and the 6-31+G(d,p) basis set for organic atoms.

Amino Acid + Monosubstituted Aqua Cisplatin → Monosubstituted Aqua Cisplatin-Amino Acid + Chloride			
	ΔE_{rxn}(kcal/mol)	**ΔH_{rxn}(kcal/mol)**	**ΔG_{rxn}(kcal/mol)**
Arginine	19.60275	22.3594	30.22836
Aspartate	-0.07907	0.599899	7.600389
Cysteine	-14.776	-13.2712	-8.90498
Glutamate	-0.2574	0.557856	6.688681
Histidine-Nε	19.82847	20.74087	27.92478
Histidine-Nδ	27.73998	29.22623	35.58786
Lysine	-5.7156	-3.15455	3.548814
Methionine	2.941762	4.631707	12.07905

Table 2. Calculated Thermodynamics for amino acid binding monosubstituted cisplatin. Inputs were modeled in Avogadro 2 and then geometrically optimized with a frequency calculation in ORCA via the restricted B3YLP method using a def2-TZVP basis set for platinum atoms and the 6-31+G(d,p) basis set for organic atoms.

Amino Acid + Disubstituted Aqua Cisplatin → Monosubstituted Aqua Cisplatin-Amino Acid + H_2O			
	ΔE_{rxn}(kcal/mol)	**ΔH_{rxn}(kcal/mol)**	**ΔG_{rxn}(kcal/mol)**
Arginine	4.208075	4.759028	9.843734
Aspartate	-15.4737	-17.0005	-12.7842
Cysteine	-30.1706	-30.8716	-29.2896
Glutamate	-15.6521	-17.0425	-13.6959
Histidine-Nε	4.43379	3.140494	7.540148
Histidine-Nδ	12.3453	11.62586	15.20323
Lysine	-21.1103	-20.7549	-16.8358
Methionine	-12.4529	-12.9687	-8.30558

Table 3. Calculated thermodynamics for amino acid binding disubstituted cisplatin Inputs were modeled in Avogadro 2 and then geometrically optimized with a frequency calculation in ORCA via the restricted B3YLP method using a def2-TZVP basis set for platinum atoms and the 6-31+G(d,p) basis set for organic atoms.

Studying Protein-Cisplatin Interactions with Molecular Docking

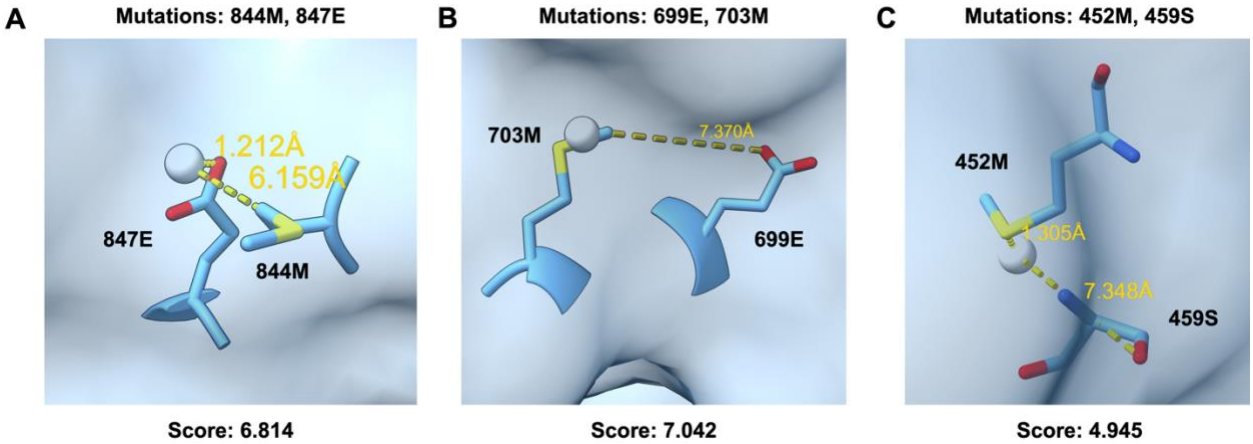

Figure 3. Docking of Pt^{2+} Against the Human MutSα Complex. The MIB2 web server was used to dock Pt^{2+} to MutSα, computing mutations at (A) 844M and 847E, (B) 699E and 703, and (C) 452M and 459S. Atomic distances from platinum to the residues are shown.

Over time, cisplatin has been adapted into numerous platinum-containing derivatives with significantly different structures. To investigate how platinum, as an ion, interacts with proteins, we used MIB2: Metal Ion-Binding site prediction and modeling server to investigate platinum binding from a whole-protein perspective[19]. We docked Pt^{2+} against the MSH6 crystal structure and obtained binding scores for 23 different Pt^{2+} binding sites (see **Supplemental Information, Table S1**). The individual acids consistently present in high-scoring binding sites are glutamate, methionine, and aspartate. The highest-scoring site involved coordination of lysine and methionine in a planar geometry (**Figure 3**). The next-highest-scoring site involved coordination between methionine and glutamate, and the third-highest was between two methionine residues. Both calculations for amino acid-cisplatin binding and Pt^{2+} docking show interactions of glutamate, methionine, and aspartate to be very favorable. We hypothesize that such interactions could be driven by the platinum ion.

After observing how amino acids coordinate cisplatin and how protein binding sites coordinate platinum ions, we wanted to investigate how cisplatin binds at the protein level. We chose MSH6 as a model protein with a cisplatin-binding site, (5) due to MSH6 causing DNA contortion upon binding, exposing both guanine and thymine for potential alteration. From our model of DNA binding by the MutSα complex, we observed a favorable proximity of the protein binding site to purine-containing nucleobases (**Figure 4**).

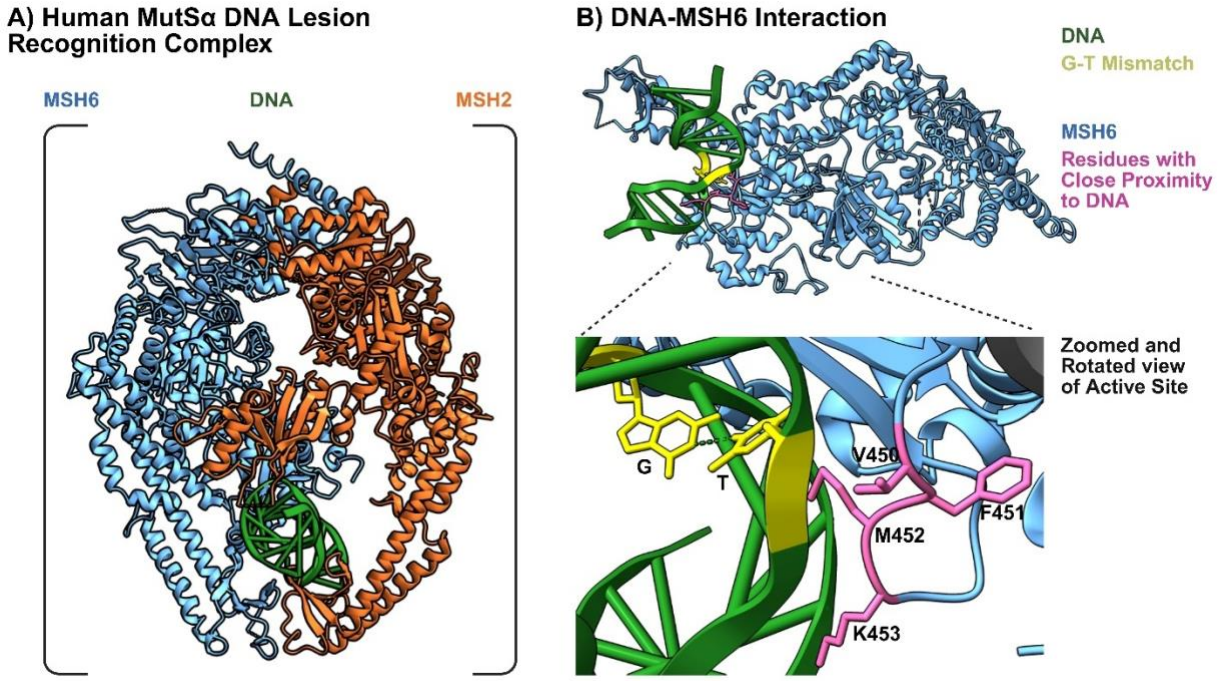

Figure 4. The Human MutSα Complex (MSH2/MSH6). (A) A DNA-lesion recognition complex that (B) is sensitive to Guanine-Thymine base pair mismatches, PDB: (2O8B). Molecular visualization was performed with ChimeraX.

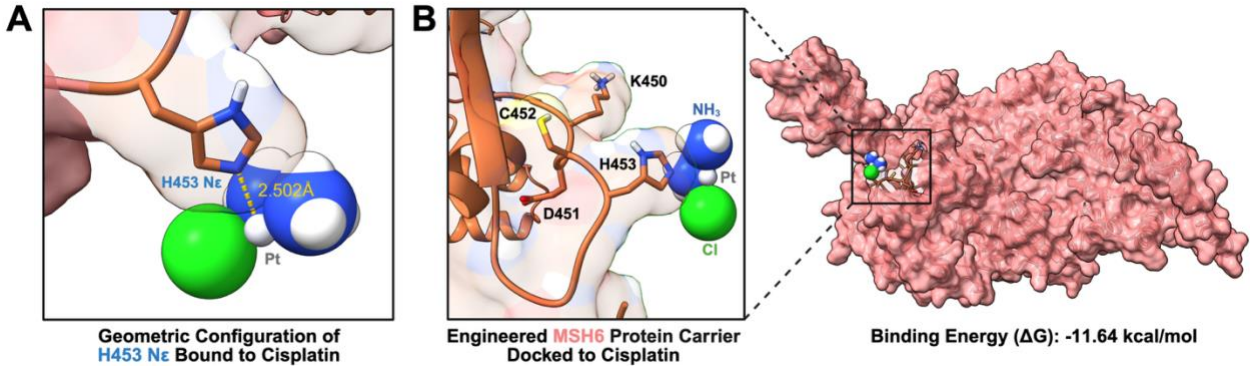

Figure 5. Molecular docking of cisplatin to engineered MSH6. Mutagenesis was performed on the MSH6 crystal structure (PDB: 2O8B), specifically residues V450K, F451D, M452C, K453H. MetalDock was used to dock (A) the geometric configuration of the Nε to the Pt2+ in cisplatin. (B) The engineered protein carrier is visualized in a thermodynamically stable pose, as quantified by the binding energy (ΔG) of -11.64 kcal/mol.

We used MetalDock to dock cisplatin to the engineered binding site of engineered MSH6. The most favorable docking position was measured to have a binding energy of -11.64 kcal/mol, and

the average of ten runs was -11.57 kcal/mol. Cisplatin coordinated Histidine-Nε (**Figure 5**). This insight was unexpected, as cysteine, lysine, and aspartate were each present within the site, and where these candidate binding residues were calculated to have a higher affinity for the platinum compound. However, this result aligns with recent observations from experimental structures, as histidine is among the most common cisplatin binders in the Protein Data Bank[13]. Another surprising observation was that cisplatin did not adopt a square-planar geometry within our most energetically favorable poses in the coordination and binding model. However, coordination could still be accounted for: the input cisplatin file coordinated two chlorines, whereas the output file coordinated only one.

Predictive Analysis of the Structural Impact of Inserting Cisplatin-Binding Site

We chose to insert the cisplatin-binding site into residues 450-453 of MSH6 because of its proximity to DNA within the MutSα complex. Additionally, this site is optimal because it is a loop rather than a part of the backbone secondary structure. Therefore, we hypothesized that mutagenesis of residues 450-453 would preserve the remaining MSH6 structure. To test this, we used Chai-1 with the MSH6 crystal structure template and Boltz-2 without a template to predict the structure of engineered MSH6 (**Figure 6**). Following this, the engineered MSH6 predictions and the complete MSH6 crystal structure were aligned in Chimera[20]. The alignment score for the crystal structure against the Chai-1 predicted MSH6 was 4623.6, and the predicted Boltz-2 alignment was 4624.1 using the mutated ligand sequence outlined by residues 450-453.

When observing the active sites of each alignment, they appear to be consistent with the crystal structure, while inconsistencies appear farther from the binding site. Because of this, we believe that structural differences are more likely a result of imperfect structural prediction rather than being inflected by mutagenesis. Another possible reason could be gaps in the crystal structure that could not be accounted for during structural prediction. To validate this claim, we repeated the structural prediction procedures using an unmutated MSH6 sequence. Here, we found that the predicted wild-type MSH6 showed closer alignment with the predicted structure of mutated MSH6 than with the crystal structure, supporting the idea that inconsistencies are due to imperfect structural prediction rather than errors in the protein sequence (see **Supplemental Information, Tables S2,S3**). Additionally, we repeated this process with Boltz-2 and had difficulty using the MSH6 crystal structure as a template. Specifically, predictions for both wild-type and engineered MSH6 were highly unlike the crystal structure at the C-terminus. However, the binding site and the N-terminal region around it were found to yield a better overall alignment, consistent with the

observation that mutagenesis of residues 450-453 has little impact on the rest of the MSH6 structure. The unmutated and each of the mutated MSH6 proteins were predicted by Expasy ProtParam to have a long half-life in bacteria, yeast, and mammalian cells. This provides initial evidence that these mutations do not significantly affect the stability or the compatibility with recombinant expression of MSH6 (see **Supplemental Information, Table S5**). Although in this study MSH6 was mutated to bind a chemotherapeutic payload, MSH6 alone does not exhibit tumor specificity.

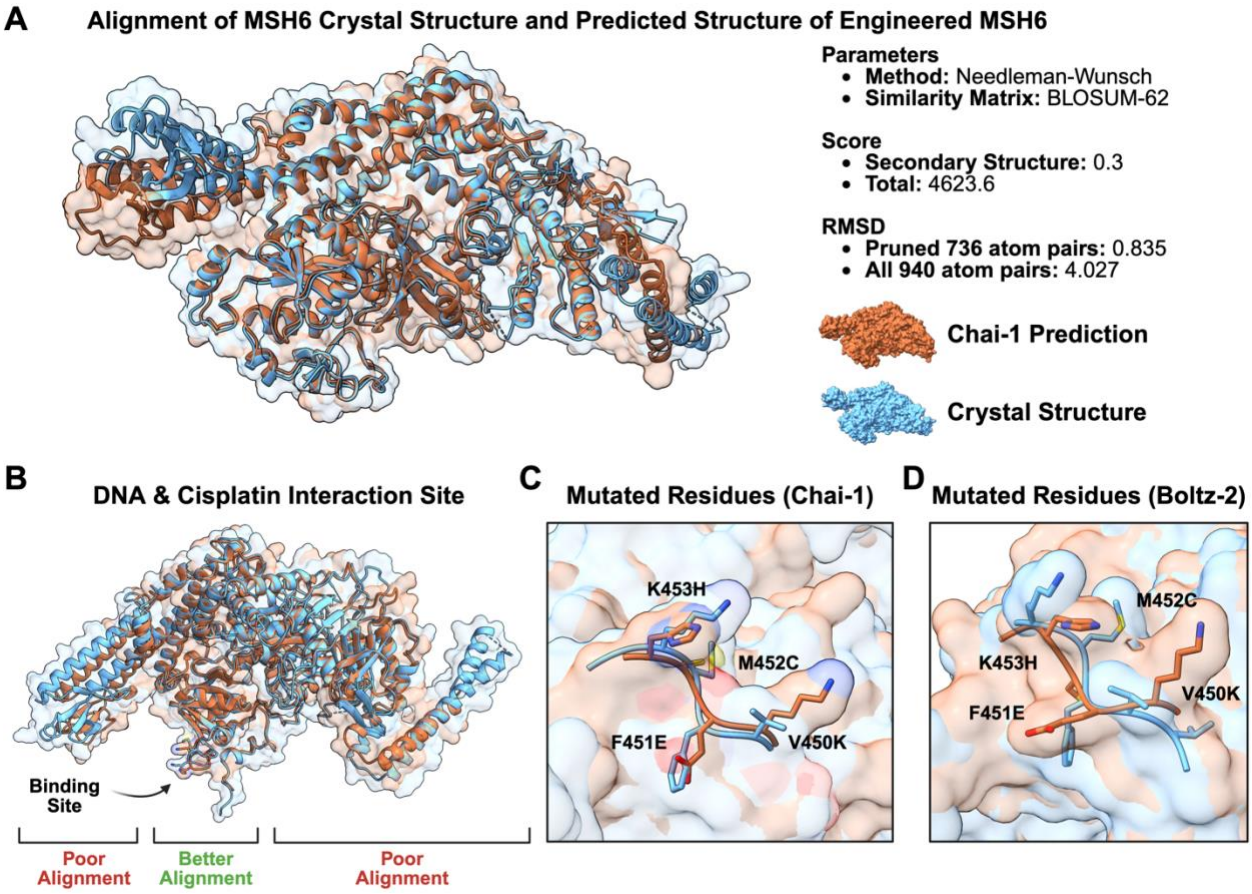

Figure 6. Alignment of the MSH6 crystal structure to structural predictions of engineered MSH6. (A) Alignment of the full MSH6 crystal structure to the structural prediction of engineered MSH6, using Chai-1. (B) Alignment of the Chai-1 predicted structure and the crystal structure, with better alignment at the cisplatin active site. A region of the protein-DNA interaction binding site (residues 450-453) was mutated to visualize the predicted shift in protein structure and potential binding affinity to cisplatin.

Confirm and Reveal the Mechanism of Action of Cisplatin with DNA

Cisplatin carries out its chemotherapeutic action by crosslinking two purine bases on a DNA strand, causing irreparable damage that leads to cell death. Many biochemical, biophysical, and structural studies indicate that crosslinking is the primary interaction of cisplatin with DNA. We used density functional theory methods to study amino acid-cisplatin binding to investigate the thermodynamics behind nucleobase-cisplatin binding.

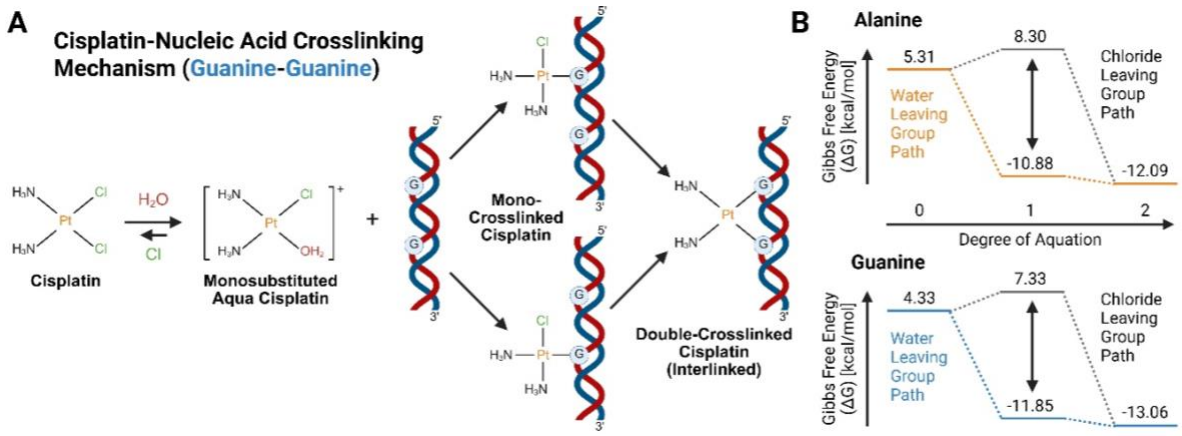

Figure 7. Geometrically Optimized Nucleic Acid Aquation and DNA Crosslinking. (A) Reactions associated with (A) adenine and (B) guanine driven aquation of cisplatin, yielding a monosubstituted cisplatin complex.

Cisplatin undergoes aquation upon entering the cell, and it has been reported that the second aquation step occurs while bound to one nucleotide[21]. Therefore, initially, monosubstituted cisplatin binds a nucleotide while kicking off a water ion, after which it undergoes a second aquation step before removing the chloride ion. The process of cisplatin crosslinking DNA has been thoroughly investigated both experimentally and computationally. By calculating the monosubstituted aqua-cisplatin interactions, we quantified the thermodynamics for each of the two possible reaction schemes. Here, we found that water was a favorable leaving group, whereas chlorine was an unfavorable one, and that the binding of disubstituted cisplatin was slightly more thermodynamically favorable (**Figure 7**). Next, cisplatin crosslinking purine bases were modeled and thermodynamically investigated (**Tables 4-8**). Cisplatin crosslinking of two guanine bases was calculated to be the most thermodynamically favorable reaction, consistent with experimental findings[22]. Here, we also quantified the thermodynamics of adenine crosslinking to guanine (**Figure 8**). In this model, we found that guanine binding is significantly better than that of adenine, again consistent with previously reported models and experiments[22] .

Nucleobase + Cisplatin → Cisplatin-Nucleobase + Chloride			
	ΔE_{rxn}(kcal/mol)	**ΔH_{rxn}(kcal/mol)**	**ΔG_{rxn}(kcal/mol)**
Adenine	-1.86031	-0.99824	5.307973
Guanine	-2.91233	-1.51336	4.328181

Table 4. Computationally derived thermodynamics for nucleobases binding cisplatin. Inputs were modeled in Avogadro 2 and then geometrically optimized with a frequency calculation in ORCA via the restricted B3YLP method using a def2-TZVP basis set for platinum atoms and the 6-31+G(d,p) basis set for organic atoms.

Nucleobase + Monosubstituted Aqua Cisplatin → Monosubstituted Aqua Cisplatin-Nucleobase + Chloride			
	ΔE_{rxn}(kcal/mol)	**ΔH_{rxn}(kcal/mol)**	**ΔG_{rxn}(kcal/mol)**
Adenine	1.135478	2.054213	8.297991
Guanine	-0.36244	0.37702	7.326431

Table 5. Computationally derived thermodynamics for nucleobases binding monosubstituted cisplatin. Inputs were modeled in Avogadro 2 and then geometrically optimized with a frequency calculation in ORCA via the restricted B3YLP method using a def2-TZVP basis set for platinum atoms and the 6-31+G(d,p) basis set for organic atoms.

Nucleobase + Monosubstituted Aqua Cisplatin → Cisplatin-Nucleobase + H_2O			
	ΔE_{rxn}(kcal/mol)	**ΔH_{rxn}(kcal/mol)**	**ΔG_{rxn}(kcal/mol)**
Adenine	-13.66	-14.8674	-10.8736
Guanine	-14.712	-15.3826	-11.8534

Table 6. Computationally derived thermodynamics for nucleobases binding monosubstituted cisplatin. Inputs were modeled in Avogadro 2 and then geometrically optimized with a frequency calculation in ORCA via the restricted B3YLP method using a def2-TZVP basis set for platinum atoms and the 6-31+G(d,p) basis set for organic atoms.

Nucleobase + Disubstituted Aqua Cisplatin → Monosubstituted Aqua Cisplatin-Nucleobase + H_2O			
	ΔE_{rxn}(kcal/mol)	**ΔH_{rxn}(kcal/mol)**	**ΔG_{rxn}(kcal/mol)**
Adenine	-14.2592	-15.5462	-12.0866
Guanine	-15.7571	-17.2234	-13.0582

Table 7. Computationally derived thermodynamics for nucleobases binding disubstituted cisplatin. Inputs were modeled in Avogadro 2 and then geometrically optimized with a frequency calculation in ORCA via the restricted B3YLP method using a def2-TZVP basis set for platinum atoms and the 6-31+G(d,p) basis set for organic atoms.

2 *Nucleobases* + *Disubstituted Aqua Cisplatin* → *Nucleobase-Cisplatin-Nucleobase* + 2 H_2O			
	ΔE_{rxn}(kcal/mol)	**ΔH_{rxn}(kcal/mol)**	**ΔG_{rxn}(kcal/mol)**
Adenine-Cisplatin-Adenine	-27.8521	-28.5445	-21.205
Adenine-Cisplatin-Guanine	-30.3336	-31.382	-24.361
Guanine-Cisplatin-Guanine	-30.5517	-31.7321	-25.1664

Table 8. Computationally derived thermodynamics for cisplatin crosslinking nucleobases. Inputs were modeled in Avogadro 2 and then geometrically optimized with a frequency calculation in ORCA via the restricted B3YLP method using a def2-TZVP basis set for platinum atoms and the 6-31+G(d,p) basis set for organic atoms.

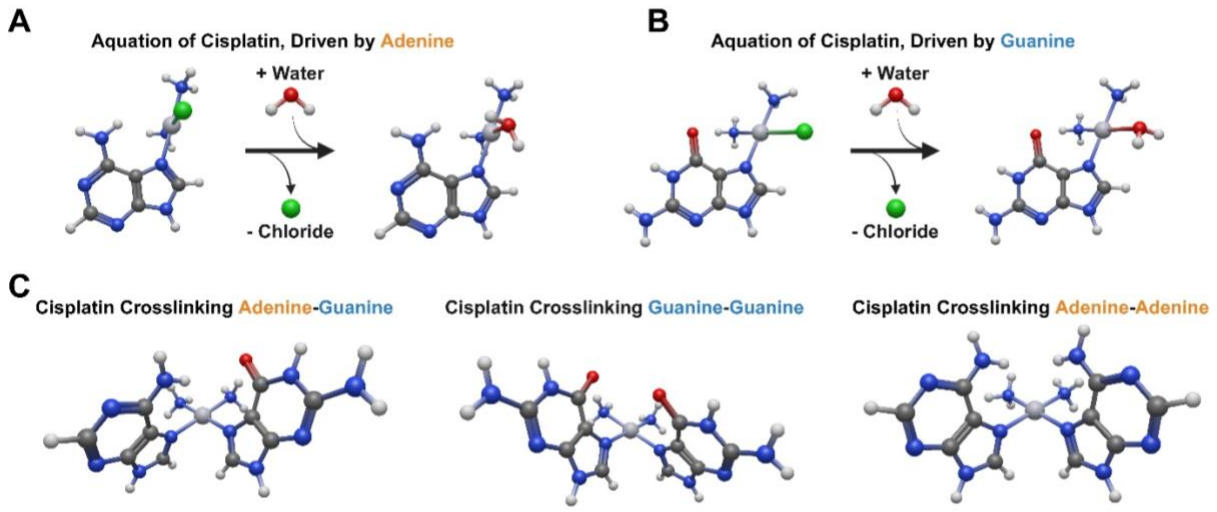

Figure 8. Geometrically Optimized Nucleic Acid Aquation and DNA Crosslinking. (A) Reactions associated with (A) adenine and (B) guanine driven aquation of cisplatin, yielding a monosubstituted cisplatin complex. (C) Cisplatin crosslinks two nucleic acids from the monosubstituted complex. Input and output structures were modeled in Avogadro 2. Geometry optimization was performed with ORCA via the restricted B3YLP method using a def2-TZVP basis set for platinum atoms and the 6-31+G(d,p) basis set for organic atoms.

Conclusion

In this work, we evaluated the mechanism of action of cisplatin, from its coordination with a model protein carrier to its reaction with nucleic acids, quantifying the energetics and thermodynamics of cisplatin binding. Our docking studies of engineered human MSH6 reveal preferential cisplatin binding to histidine, where the binding pocket contains cysteine, glutamate, and lysine residues as key neighbors of the cisplatin complex. These results are surprising compared to DFT calculations of amino acids, which showed a stable, preferential sulfur-based platinum coordination with cysteine. The cysteine coordination was the strongest among the amino acids, regardless of the cisplatin aquation state. This observation of high-affinity capture to cysteine is consistent with previous experimental reports that cysteine is a preferred amino acid for covalent adduct formation[22]. A potential reason why our cysteine residue didn't coordinate cisplatin is its orientation. Future work can repeat this protocol, but with amino acid residue positions swapped.

Further, we considered the potential for nitrogen-based coordination chemistries, hypothesizing that coordination to histidine is tunable depending on the nitrogen-binding site and the degree of

aquation. Recognizing that histidine shares a functional group with the purine group in known nucleobase binders of cisplatin, providing a potential analogue for understanding thermodynamic differences in cisplatin coordination to the delta and epsilon nitrogen atoms of histidine. Balancing stability during transport to the cell via proteins and release within the cell, histidine provides a novel strategy to modulate the strength of the protein-cisplatin interaction, thereby enhancing cellular uptake and increasing the rate of release from the protein within the cell. Once inside the cell and unbound from the protein carrier, we observed a strong thermodynamic drive for cisplatin to crosslink DNA, consistent with previous reports. Specifically, we found that for purine-containing nucleobases (i.e., adenine and guanine), the disubstituted aquation complex of cisplatin is most thermodynamically favorable. Among the nucleobases, we observed that guanine preferentially binds to adenine, and the bridged cisplatin-guanine-guanine complex was the most favorable configuration, reinforcing the mechanistic endpoint that cisplatin aquation is thermodynamically most favorable for nucleic-acid modification.

Discussion

These results provide a rational path from amino acid energetics to the design of active sites within protein candidates for chemotherapy delivery. Here, these active sites can be mutated to modulate cisplatin binding affinity by tuning the rate of aquation, altering structural accessibility within the carrier scaffold, and orienting cysteine or histidine residues (as sulfur vs nitrogen donors) at the site, thereby strengthening the protein-cisplatin interaction and enhancing cellular uptake. While high-affinity chemistries are sought after in the protein-drug conjugate field, a balancing act may be required for optimal targeted delivery of cisplatin, in which stable loading of the platinum coordinator should be balanced with kinetic trapping (i.e., premature sequestration) in off-target proteins. While cysteine is traditionally the active-site binder of cisplatin, forming a histidine-centered coordination of cisplatin offers a unique strategy to build carriers that enhance the circulation half-life and tumor delivery of cisplatin from systemic administration, while still allowing rapid aquation upon release from the protein carrier and DNA adduct formation.

Future studies can build off this work by creating a fusion construct between MSH6 and a delivery protein, such as an antibody or nanobody[23,24]. Fusion proteins have recently shown success in localizing enzyme function in $HER2^+$ breast cancer mouse models[25] and in selectively delivering STING-pathway-activating proteins[26,27]. Further, in the design of protein carriers, it is important to recognize that the modeled protein, MSH6, may have limited transport properties after

administration due to its size and solubility, even when fused to a nanobody. In that event, knowledge of cisplatin-binding amino acids could be applied to install a platinum-drug-binding site into a different or artificial protein scaffold. We expect that, from these results, rational protein design will play a key role in creating tunable cisplatin-binding sites within optimal protein carriers for low-toxicity, tumor-specific delivery (e.g., engineered nanobodies for high-affinity tumor delivery)[27–29] and in offering a strategy for integrating an expanded library of cisplatin derivatives.

References

1. Mariconda, A. *et al.* Cisplatin, the Timeless Molecule. *Inorganics* **13**, 246 (2025).
2. Romani, A. M. P. Cisplatin in cancer treatment. *Biochemical Pharmacology* **206**, 115323 (2022).
3. Liu, B., Zhou, H., Tan, L., Siu, K. T. H. & Guan, X.-Y. Exploring treatment options in cancer: tumor treatment strategies. *Sig Transduct Target Ther* **9**, 175 (2024).
4. Luo, L.-Z., Jin, H.-W. & Huang, H.-Q. Transferrin–cisplatin specifically deliver cisplatin to HepG2 cells in vitro and enhance cisplatin cytotoxicity. *Journal of Proteomics* **77**, 237–250 (2012).
5. Peng, H., Jin, H., Zhuo, H. & Huang, H. Enhanced antitumor efficacy of cisplatin for treating ovarian cancer *in vitro* and *in vivo* via transferrin binding. *Oncotarget* **8**, 45597–45611 (2017).
6. Safaei, R., Otani, S., Larson, B. J., Rasmussen, M. L. & Howell, S. B. Transport of Cisplatin by the Copper Efflux Transporter ATP7B. *Molecular Pharmacology* **73**, 461–468 (2008).
7. Warren, J. J. *et al.* Structure of the Human MutSα DNA Lesion Recognition Complex. *Molecular Cell* **26**, 579–592 (2007).
8. Hanwell, M. D. *et al.* Avogadro: an advanced semantic chemical editor, visualization, and analysis platform. *J Cheminform* **4**, 17 (2012).
9. Neese, F. The ORCA program system. *WIREs Comput Mol Sci* **2**, 73–78 (2012).
10. Neese, F. Software Update: The ORCA Program System—Version 6.0. *WIREs Comput Mol Sci* **15**, e70019 (2025).
11. Stephens, P. J., Devlin, F. J., Chabalowski, C. F. & Frisch, M. J. Ab Initio Calculation of Vibrational Absorption and Circular Dichroism Spectra Using Density Functional Force Fields. *J. Phys. Chem.* **98**, 11623–11627 (1994).
12. Baugh, E. H., Lyskov, S., Weitzner, B. D. & Gray, J. J. Real-Time PyMOL Visualization for Rosetta and PyRosetta. *PLoS ONE* **6**, e21931 (2011).
13. Tanley, S. W. M. & Helliwell, J. R. Structural dynamics of cisplatin binding to histidine in a protein. *Structural Dynamics* **1**, 034701 (2014).
14. Boal, A. K. & Rosenzweig, A. C. Crystal Structures of Cisplatin Bound to a Human Copper Chaperone. *J. Am. Chem. Soc.* **131**, 14196–14197 (2009).
15. Zimmermann, T., Chval, Z. & Burda, J. V. Cisplatin Interaction with Cysteine and Methionine in Aqueous Solution: Computational DFT/PCM Study. *J. Phys. Chem. B* **113**, 3139–3150 (2009).

16. Chiaverini, L. *et al.* Mechanistic Fingerprints from Chloride to Iodide: Halide vs. Ammonia Release in Platinum Anticancer Complexes. *IJMS* **26**, 12138 (2025).
17. Ferraro, G., Ciambellotti, S., Messori, L. & Merlino, A. Cisplatin Binding Sites in Human H-Chain Ferritin. *Inorg. Chem.* **56**, 9064–9070 (2017).
18. Russo Krauss, I., Ferraro, G. & Merlino, A. Cisplatin–Protein Interactions: Unexpected Drug Binding to N-Terminal Amine and Lysine Side Chains. *Inorg. Chem.* **55**, 7814–7816 (2016).
19. Lu, C.-H. *et al.* MIB2: metal ion-binding site prediction and modeling server. *Bioinformatics* **38**, 4428–4429 (2022).
20. Meng, E. C. *et al.* UCSF CHIMERAX : Tools for structure building and analysis. *Protein Science* **32**, e4792 (2023).
21. Rocha, C. R. R., Silva, M. M., Quinet, A., Cabral-Neto, J. B. & Menck, C. F. M. DNA repair pathways and cisplatin resistance: an intimate relationship. *Clinics* **73**, e478s (2018).
22. Baik, M.-H., Friesner, R. A. & Lippard, S. J. Theoretical Study of Cisplatin Binding to Purine Bases: Why Does Cisplatin Prefer Guanine over Adenine? *J. Am. Chem. Soc.* **125**, 14082–14092 (2003).
23. Culkins, C. *et al.* Unlocking the Gates: Therapeutic Agents for Noninvasive Drug Delivery Across the Blood-Brain Barrier. *Mol. Pharmaceutics* **21**, 5430–5454 (2024).
24. Slaton, E. W., Clay, N., Phan, N. & Kimmel, B. R. Innovations in Yeast Synthetic Biology: Engineered Discovery Systems for Immunotherapy. *ACS Synth. Biol.* **14**, 3293–3305 (2025).
25. Metcalf, K. J. *et al.* Synthetic Tuning of Domain Stoichiometry in Nanobody–Enzyme Megamolecules. *Bioconjugate Chem.* **32**, 143–152 (2021).
26. Wang-Bishop, L. *et al.* STING-activating nanoparticles normalize the vascular-immune interface to potentiate cancer immunotherapy. *Sci. Immunol.* **8**, eadd1153 (2023).
27. Kimmel, B. R. *et al.* Potentiating cancer immunotherapies with modular albumin-hitchhiking nanobody–STING agonist conjugates. *Nat. Biomed. Eng* **9**, 1719–1739 (2025).
28. Adomanis, R., Phan, N., Walter, G. & Kimmel, B. R. Modular Nanobody Conjugates with Controlled Topology Using Genetically Encoded Non-canonical Amino Acids. Preprint at https://doi.org/10.1101/2025.11.27.691038 (2025).
29. Chen, Y. *et al.* Molecular Matchmakers: Bioconjugation Techniques Enhance Prodrug Potency for Immunotherapy. *Mol. Pharmaceutics* **22**, 58–80 (2025).

AUTHOR INFORMATION

Corresponding Author

Blaise R. Kimmel, Ph.D.

151 W. Woodruff Avenue

Columbus, OH 43210

Email: kimmel.85@osu.edu

Author Contributions

Soren Spina: Wrote the original draft of the manuscript, generated all figures and graphics for the manuscript, edited, revised, and approved the final version of the manuscript. Joe Bailey: Supported data generation for the manuscript and figure preparation. Blaise Kimmel: Edited, revised, and approved the final version of the manuscript, and acquired funding to support the work.

Funding Sources

We gratefully thank the Ohio State University Comprehensive Cancer Center (OSUCCC), OSUCCC Center for Cancer, and the Department of Chemical and Biomolecular Engineering at The Ohio State University for support of this work.

Conflicts of Interest

The authors declare no competing financial interests.

Acknowledgements

This work was supported in part by The Ohio State University Center for Cancer Engineering-Curing Cancer Through Research in Engineering and Sciences. B.R.K. acknowledges financial support from the Prostate Cancer Foundation Young Investigator Award. All figures created with Biorender.com.

Supplementary Information

Table S1. Prediction Scoring of 23 different Pt^{2+} binding sites.

No.	Binding Residues	Template	Score
1	1140K, 1144M	4lq6A0	8.181
2	699E, 703M	4lq6A0	7.042
3	844M, 847E	3m7kA0	6.814
4	452M, 459S	4lq6A0	4.945
5	934D, 936D, 937Y	6mw5A0	4.625
6	665E, 667D	6mw5A0	4.587
7	580S, 1202M	5mu1A2	4.224
8	544E, 601L	4pkeA0	4.007
9	703M, 826H	4dpeA0	3.98
10	826H, 1042K	6aqkA0	3.544
11	392D, 394S	6ig4A0	3.503
12	380D, 381E	6ig4A0	3.107
13	547E, 550S	6ig4A0	3.027
14	562D, 564S	6ig4A0	3.025
15	839D, 844M	4dpeA0	2.893
16	380D, 382H, 383R	6mw5A0	2.835
17	576D, 578H, 581R	6mw5A0	2.814
18	826H, 830S	6fhnA1	2.709
19	1250H, 1254E	4pm3A0	2.64
20	1080L, 1119E	1rnlA0	2.496
21	833K, 837H	3w3sA0	2.477
22	761R, 1153M	4ombC0	2.338
23	629D, 631S	6ig4A0	2.3313

Table S2: Sequences of MSH6 (Blue are sites of mutagenesis, yellow is mutagenesis).

MSH6	MSRQSTLYSFFPKSPALSDANKASARASREGGRAAAAPGASPSPGGDAAWSE AGPGPRPLARSASPPKAKNLNGGLRRSVAPAAPTSCDFSPGDLVWAKMEGYP WWPCLVYNHPFDGTFIREKGKSVRVHVQFFDDSPTRGWVSKRLLKPYTGSKSK EAQKGGHFYSAKPEILRAMQRADEALNKDKIKRLELAVCDEPSEPEEEEEMEVG TTYVTDKSEEDNEIESEEEVQPKTQGSRRSSRQIKKRRVISDSESDIGGSDVEFK PDTKEEGSSDEISSGVGDSESEGLNSPVKVARKRKRMVTGNGSLKRKSSRKET PSATKQATSISSETKNTLRAFSAPQNSESQAHVSGGGDDSSRPTVWYHETLEW LKEEKRRDEHRRRPDHPDFDASTLYVPEDFLNSCTPGMRKWWQIKSQNFDLVI CYKVGKFYELYHMDALIGVSELGLVFMKGNWAHSGFPEIAFGRYSDSLVQKGYK VARVEQTETPEMMEARCRKMAHISKYDRVVRREICRIITKGTQTYSVLEGDPSE NYSKYLLSLKEKEEDSSGHTRAYGVCFVDTSLGKFFIGQFSDDRHCSRFRTLVA HYPPVQVLFEKGNLSKETKTILKSSLSCSLQEGLIPGSQFWDASKTLRTLLEEEY FREKLSDGIGVMLPQVLKGMTSESDSIGLTPGEKSELALSALGGCVFYLKKCLID QELLSMANFEEYIPLDSDTVSTTRSGAIFTKAYQRMVLDAVTLNNLEIFLNGTNGS TEGTLLERVDTCHTPFGKRLLKQWLCAPLCNHYAINDRLDAIEDLMVVPDKISEV VELLKKLPDLERLLSKIHNVGSPLKSQNHPDSRAIMYEETTYSKKKIIDFLSALEGF KVMCKIIGIMEEVADGFKSKILKQVISLQTKNPEGRFPDLTVELNRWDTAFDHEKA RKTGLITPKAGFDSDYDQALADIRENEQSLLEYLEKQRNRIGCRTIVYW
MSH6 Mutated Region Mut: Arg	PTVWYHETLEWLKEEKRRDEHRRRPDHPDFDASTLYVPEDFLNSCTPGMRKW WQIKSQNFDLVICYKVGKFYELYHMDALIGVSELGLKECHGNWAHSGFPEIAFG RYSDSLVQKGYKVARVEQTETPEMMEARCRKMAHISKYDRVVRREICRIITKGT QTYSVLEGDPSENYSKYLLSLKEKEEDSSHTRAYGVCFVDTSLGKFFIGQFSDD RHCSRFRTLVAHYPPVQVLFEKGNLSKETKTILKSSLSCSLQEGLIPGSQFWDAS KTLRTLLEEEYFREKLSDGIVMLPQVLKGMTSESDSIGLTPGEKSELALSALGGC VFYLKKCLIDQELLSMANFEEYIPLDSDTVSKAYQRMVLDAVTLNNLEIFLNGTNG STEGTLLERVDTCHTPFGKRLLKQWLCAPLCNHYAINDRLDAIEDLMVVPDKISE VVELLKKLPDLERLLSKIHNVGSPLKSQNHPDSRAIMYEETTYSKKKIIDFLSALEG FKVMCKIIGIMEEVADGFKSKILKQVISLQTKNPEGRFPDLTVELNRWDTAFDHEK ARKTGLITPKAGFSDYDQALADIRENEQSLLEYLEKQRNRIGCRTIVYWGIGRNR YQLEIPENFTTRNLPEYELKSTKKGCKRYWTKTIEKKLANLINAEERRDVSLKDC MRRLFYNFDKNYKDWQSAVECIAVLDVLLCLANYSRGGDGPMCRPVILLPEDTP PFLELKGSRHPCGDDFIPNDILIGCEEEEQKAYCVLVTGPNMGGKSTLMRQAGL LAVMAQMGCYVPAEVCRLTPIDRVFTRLGSTFFVELSETASILMHATAHSLVLVD ELGRGTATFDGTAIANAVVKELAETIKCRTLFSTHYHSLVEDYSQNVAVRLGHMA CMTFLYKFIKGACPKSYGFNAARLANLPEEVIQKGHRKAREFEKMNQSLRLFRE

Table S3. Prediction Scoring Boltz-2.

MSH6	**confidence_score**	**ptm**
Wild-Type	0.662	0.628
Arg	0.638	0.624
Cys	0.638	0.626

Table S4. Crystal and Computationally Predicted Structures of Wild-Type & Mutated MSH6.

MSH6	Structure	Active Site
MSH6 Crystal Structure PDB: 2O8B	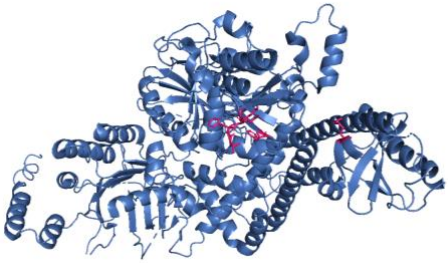	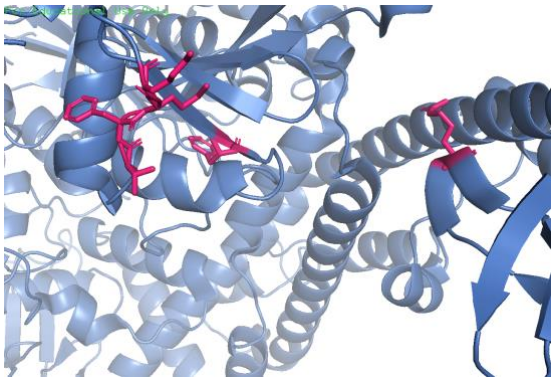
MSH6 Prediction Wild-Type	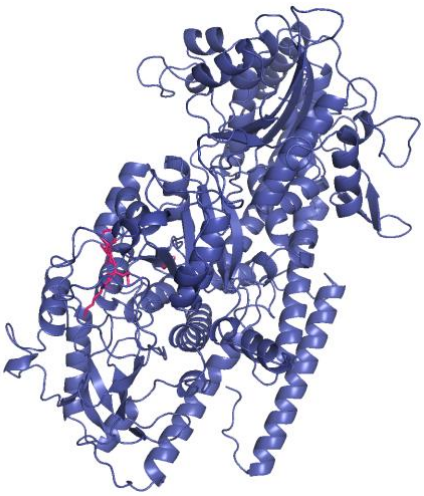	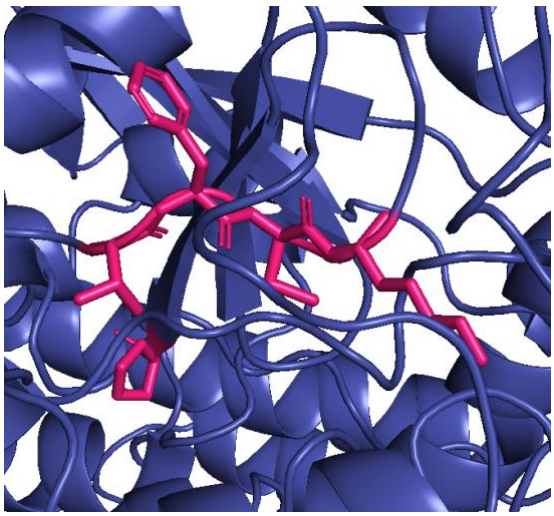
MSH6 Prediction Mut: Cys	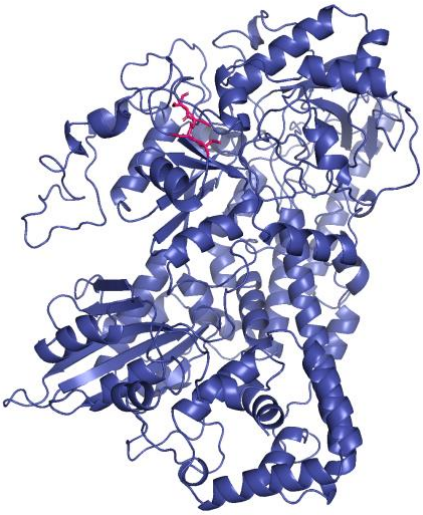	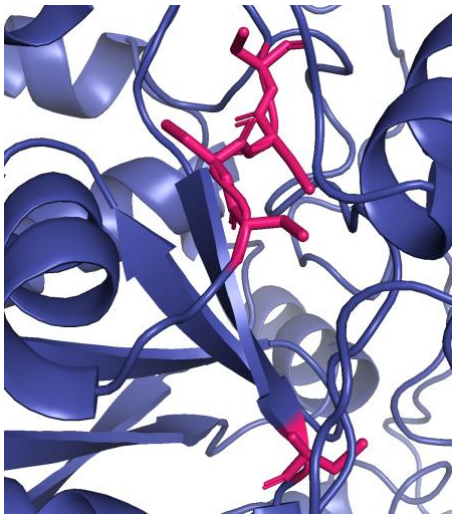

MSH6 Prediction Mut: Arg	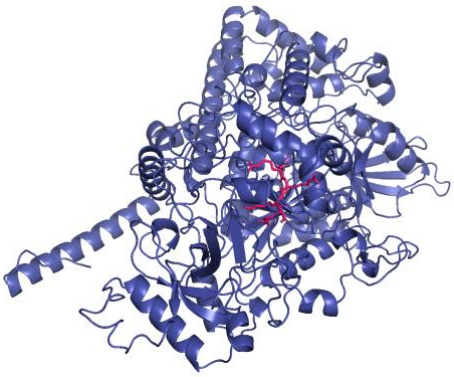	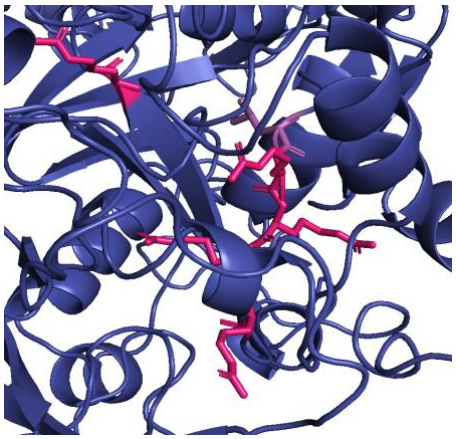

The crystal structure of MSH6 (PDB: 2O8B), along with the Boltz-2 predicted structures of each cystine-mutated and arginine-mutated MSH6 protein, was visualized in PyMOL. MSH6 is colored blue, and the five mutated residues are colored red.

Table S5. Predicted Experimental Features of the Wild-Type and Mutant MSH6 Protein.

MSH6	**Theoretical pI**	**Half-Life Mammalian**	**Half-Life Yeast**	**Half-Life Bacterial**
Wild-Type	6.5	30	>20	>10
Mut: Cys	6.31	30	>20	>10
Mut: Arg	6.74	30	>20	>10

Expasy ProtParam calculated the pI and half-life of the wild-type and mutant MSH6 proteins.

Additional Discussion of Supplemental Information

Structural predictions generated by Boltz-2 were aligned to the human MSH6 crystal structure, and each predicted structure achieved a very low alignment RMSD, indicating little similarity. As expected, the highest RMSD was observed when aligning the predicted unmutated MSH6 structure with the crystallographic model. Boltz-2 was used to predict the folding of each MSH6 protein with limited disordered regions, as shown in **Tables S2** and **S3**. In each computational prediction, although it remains near the outside environment, the active site was observed to be covered by disordered regions, closing it off from binding to DNA and possibly to platinum ligands. Meanwhile, the active site of the crystal structure was observed to be exposed for proper DNA binding.

With evidence that these sites can bind cisplatin derivatives, our goal was to determine whether mutagenesis of the DNA-interaction site preserved or disrupted the structure of MSH6 outside its active site. On the left side of every alignment, near the ATPase site of MSH6, a large section of the crystallographic model is not predicted to form by Boltz-2. Instead, these sections are predicted to fold towards the front of the image (**Table S4**), blocking residues 450-453 from interacting with either DNA or platinum compounds. The predicted structure could be the most energetically favorable, and the reason why MSH6 doesn't fold into this conformation could be through the help of a chaperone protein during initial folding. The MSH6 structure is very long and distinct because it must form a complex with MSH2. Also, the DNA-binding pocket, beyond the five amino acids of interest, carries a general positive charge that helps bind favorably to negatively charged DNA. Perhaps Boltz-2 thinks that this pocket needs to be buried within the protein core. Overall, the midsection and the region behind the active site appear to be very well conserved between the predictions and the crystal structures. This could mean that these mutations have little effect on the protein's key structural features and do not induce a major conformational change or prevent folding.